International Journal of Refrigeration 131 (2021) 146–156

Contents lists available at ScienceDirect

International Journal of Refrigeration

journal homepage: www.elsevier.com/locate/ijrefrig

Experimental parameter studies on a two-phase loop thermosyphon cooling system with R1233zd(E) and R1224yd(Z)☆

Björn Albertsen *, Gerhard Schmitz

Institute of Engineering Thermodynamics, Hamburg University of Technology, Denickestr. 17, Hamburg 21073, Germany

ARTICLE INFO

Keywords:
Two-phase loop thermosyphon
Passive cooling
Two-phase flow
R1233zd(E)
R1224yd(Z)
Electronics cooling

Mots-clés:
Thermosiphon en boucle diphasique
Refroidissement passif
Écoulement diphasique
R1233zd(E)
R1224yd(Z)
Refroidissement de composants électroniques

ABSTRACT

Two-phase loop thermosyphon (TPLT) is a promising technology looking at highly effective electronics cooling. Due to strong coupling between the internal and external parameters, in this study experimental tests in steady-state are carried out using R1233zd(E) and R1224yd(Z) as a working fluid to investigate the respective influences and resulting design requirements. The relationship between the governing thermal and flow equations is presented to facilitate the interpretation of the test results. The study shows a stable flow and cooling performance over a wide range of heat loads and recooling temperatures. The refrigerant charge is identified as one of the main influencing factors, with an optimum being between excessive subcooling and beginning dry-out. Both tested refrigerants lead to basically similar results, showing minor differences regarding thermal performance and system stability.

1. Introduction

Due to the strongly progressive electrification in many technical fields, thermal management has become one of the key challenges in engineering. Electronic components should be emphasized here, which, despite a high efficiency, emit a high heat flux because of increasing power density. High-performance cooling technologies are therefore the focus of current research, with weight playing an important role in mobile applications. Two-phase loop thermosyphon (TPLT) is one of the promising options, offering highly effective heat transfer, no power consumption and safe cooling at a low weight.

Despite the obvious advantages, this long-known technology has so far only been used widely in a few industries, such as power plants. This is because of the high sensitivity of the uncontrolled loop with regard to the boundary conditions, which makes the system design extremely difficult. For this reason there is a lot of research on the behavior of TPLTs under a wide range of operating conditions.

Khodabandeh and Palm (2000) compared experimental results from a small sized test rig with numerical calculations based on fundamental correlations of fluid dynamics to evaluate the impact of the individual pressure drops in the thermosyphon loop. In a subsequent publication the same setup was used to study the effect of the system pressure, showing increasing heat transfer coefficients for higher pressures (Khodabandeh and Palm (2002)). Copious research focuses on instability phenomena occurring in the uncontrolled system under certain operating conditions. Wu et al. (1996) identified a strong dependency of oscillations on the heat load and subcooling using a low pressure TPLT. This was also observed by Khodabandeh and Furberg (2010) as well as Nayak and Vijayan (2008) at low power and pressure during the start-up process and defined as Density-wave instability (DWI) type I. Whereas this type is characterized by backflow due to low vapor fraction, type II occurs at high heat flux with local dry-out in the evaporator. The latter could also be observed in the experimental studies of Ruppersberg and Dobson (2007) and Garrity et al. (2007). Both phenomena result in significantly reduced heat transfer coefficients. With the geysering instability Elkholy and Kempers (2020) observed another type occuring at low power using high refrigerant charges.

The refrigerant charge is a major influencing factor in two-phase thermosyphon loops, since it determines the subcooling and therefore the temperature level in the evaporator as well as the mass flow rate by the available liquid column in the downcomer. In contrast to the

☆ This article is the result of a research project funded by the Federal Ministry for Economic Affairs and Energy on the basis of a decision by the German Bundestag.
* Corresponding author.
E-mail address: bjoern.albertsen@tuhh.de (B. Albertsen).

https://doi.org/10.1016/j.ijrefrig.2021.07.036
Received 15 February 2021; Received in revised form 20 July 2021; Accepted 28 July 2021
Available online 4 August 2021
0140-7007/© 2021 The Author(s). Published by Elsevier Ltd. This is an open access article under the CC BY license (http://creativecommons.org/licenses/by/4.0/).

Nomenclature

A	cross-sectional area (m^2)
C_0	distribution factor (-)
c_{pl}	specific heat capacity of liquid at constant pressure (J/kgK)
D	diameter (m)
D_h	hydraulic diameter (m)
g	gravitational acceleration (m/s^2)
ΔH	height difference between evaporator/condenser (m)
h_{fg}	enthalpy of vaporization (kJ/kg)
L	length (m)
$\dot{G}$	mass flux (kg/m^2s)
$\dot{m}$	mass flow rate (kg/s)
Δp_{acc}	pressure difference due to acceleration (Pa)
Δp_{drive}	driving pressure difference (Pa)
Δp_{fric}	pressure difference due to friction (Pa)
Δp_{grav}	pressure difference due to gravitation (Pa)
p_{sat}	saturation pressure (Pa)
Δp_{tot}	total pressure difference (Pa)
$\dot{Q}_H$	heat load (w)
Re	Reynolds number (-)
R_{th}	thermal resistance (Kw)
T	temperature (K)
ΔT_{sub}	subcooling (K)
u	flow velocity (m/s)
u_{gi}	mean drift velocity (m/s)
x	vapor quality (kg/kg)
Greek symbols	
ϵ	void fraction (m^2/m^2)
ρ	density (kg/m^3)
Subscripts	
El	electronics surface
g	gas phase
o	homogeneous two-phase flow
i	inlet
l	liquid phase
lat	latent
m	mean value
max	maximum value
o	outlet
RC	recooling temperature
sens	sensible
Acronyms	
TPLT	two-phase loop thermosyphon

assumption of most researchers, Zhang et al. (2015b) stated that the driving force depends on the actual filling levels in the downcomer and riser tube instead of the simple height difference between condenser and evaporator. In the experimental work of Zhang et al. (2019) this is confirmed by testing large height differences up to 10m. This consideration is one of the keys to successfully building a valid system model for TPLTs (Zhang et al. (2015a)). It was also found that the refrigerant charge strongly affects the cooling performance, as a small charge can lead to dry-out, while charges which are too large result in rising subcooling due to flooding of the condenser. In their experimental work, Milanez and Mantelli (2010) confirmed the existence of an optimal refrigerant charge or rather heat transfer limit, when the downcomer is just fully filled with liquid during operation. Kang et al. (2010) showed an additional dependency of the optimal charge on the refrigerant used, which was 10% filling ratio for methanol and 30% for water. In their numerical investigation Xu et al. (2018) found the optimum lying between 20% and 30% for an evaporator with a hydrophilic surface, also using water as a refrigerant.

To evaluate the performance of a TPLT in an experimental setup Jouhara and Ezzuddin (2013) used the overall thermal resistance between the evaporator and condenser. The results in steady state showed a heat transfer characteristic typical for nucleate boiling like in other wickless evaporators. The thermal resistance was also used by Louahlia-Gualous et al. (2017) to investigate the influence of the evaporators wall roughness, showing a more effective heat transfer at low heat flux, while the values at high heat flux is not affected. Numerous different refrigerants are used for TPLTs as a working fluid, such as water, R134a, R600a, R22, HFE-7100, methanol or isobutane in the above-mentioned works. Palm and Khodabandeh (2003) compared different refrigerants by numerical simulations and gave recommendations regarding the choice of working fluid. It was found that in general the use of high pressure refrigerants leads to better performance due to higher boiling heat transfer coefficients and allows a smaller tube diameter. CO2 (R744) as an environment friendly alternative working fluid in TPLTs is investigated numerically by Zhang et al. (2017), showing that the effect of the filling ratio is stronger compared to other refrigerants, with a higher optimal charge.

Franco and Filippeschi (2012) provide a good overview of experimental works on the subject of TPLTs. They remark that certain behaviors can be observed in many experimental setups, e.g. a maximum mass flow rate as a function of the heat load, whereas the general connection between thermal and fluid dynamic has so far only been investigated insufficiently.

In this study, experimental results are presented using low-GWP refrigerants from the HFO group. In a basic TPLT setup, parameter studies are carried out to investigate the effects of heat load, recooling temperature, height difference between evaporator and condenser, refrigerant charge and refrigerant properties on the heat transfer and operating conditions. The measurements are discussed with a focus on the connection between the energy and momentum balance, and the resulting interaction between the loop parameters.

2. Experimental setup

Figure 1 shows a schematic of the test rig.

The main loop consists of four parts: evaporator, riser, condenser and downcomer. Transparent hoses are used as riser ($D = 8.8mm$, $L = 1.25m$) and downcomer ($D = 6.8mm$, $L = 1.98m$) to observe the flow pattern and the liquid column behind the condenser. The condenser is a liquid recooled plate heat exchanger with an adjustable vertical distance from the evaporator. The remaining components are used for extensive measurement of temperatures, pressures, pressure differences and mass flow rates as well as to fill and empty the system. The refrigerant charge is measured by weighing the reservoir before and after filling.

Figure 2 shows the uninsulated test rig and the evaporator assembly which is composed of the evaporator with sight glass, a heating block with four cartridges and a bracing device for setting a uniform contact pressure (hidden by the insulation).

The evaporator consists of five parallel refrigerant channels with a respective cross-sectional area of $18.28mm^2$ and a total surface area of $56.03cm^2$. The hydraulic diameter of the U-shaped channels is 4.49mm with a length of 81mm. The heating block represents the component to be cooled (e.g. power electronics) with a maximum heat load of 1.3Kw (23.2W $/cm^2$). Several thermocouples are placed near the evaporator surface and in the heating block.

The low-GWP refrigerants R1233zd(E) and R1224yd(Z) are used to reach moderate overpressure in the considered temperature range (critical points: 166.5°C, 36.2*bar*; 155.5°C, 33.4*bar*); the essential

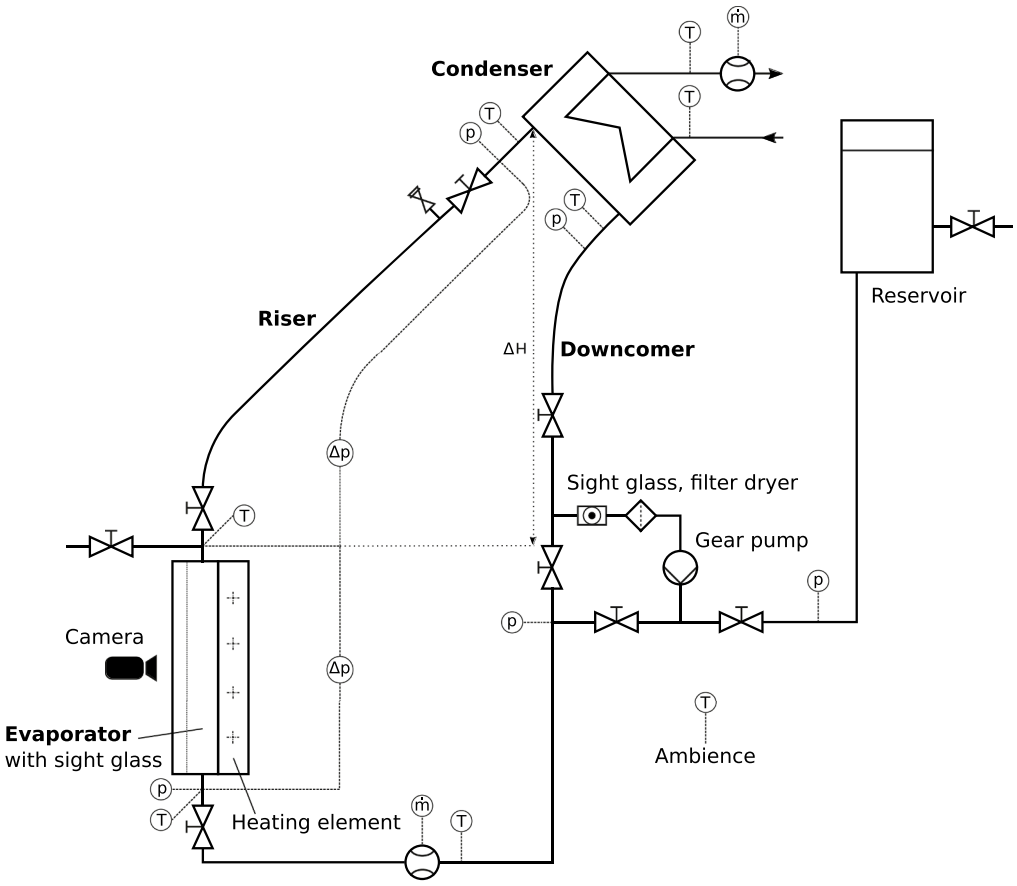

Fig. 1. Schematic of the test rig.

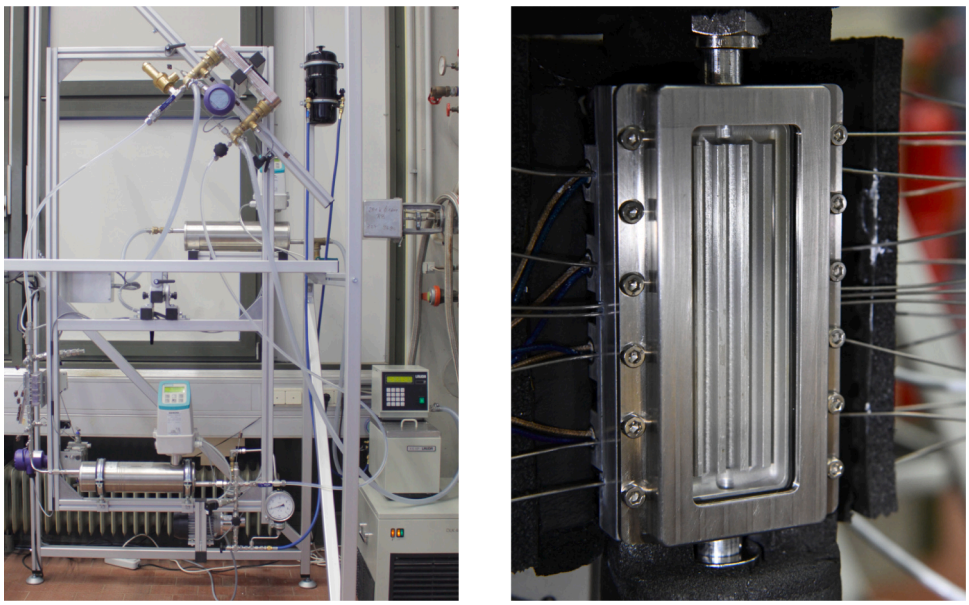

Fig. 2. Photo of the test rig and the evaporator assembly: evaporator with sight glass, heating block with cartridges, bracing device and thermocouples.

properties are listed in Table 1. The refrigerant enters the evaporator from below, is preheated, partially evaporates and flows upwards through the riser as a two-phase mixture. In the plate heat exchanger, the refrigerant completely condenses and cools down to the recooling temperature. Finally, the fully or partially liquid-filled downcomer closes the loop. The ambient temperature is 20°C during all tests. The measuring sensors used and the related uncertainties are listed in Table 2. The uncertainty propagation results for parameters calculated

Table 1
Properties of R1233zd(E) and R1224yd(Z) at temperatures of 20°C and 60°C (Lemmon et al. (2018)).

	R1233zd(E)		R1224yd(Z)	
Property	20°C	60°C	20°C	60°C
Saturation pressure p_{sat} in *bar*	1.08	3.90	1.24	4.41
Enthalpy of vaporization h_{fg} in kJ/kg	193.7	171.2	166.4	145.2
Density (liquid) ρ in kg/m^3	1275	1173	1375	1257
Spec. heat capacity (liq.) c_{pl} in J/kgK	1208	1283	1127	1218

Table 2
Measurement sensors with related uncertainties.

Measured quantity	Sensor type / measuring principle	Measurement uncertainty
Temperature (loop, recooling)	Pt100, 1/10 DIN B	$\pm(0.03 + 0.0005 \cdot T)$°C
Temperature(evaporator, heating block)	Thermocouple, type T, class 1	$\pm 0.5K$
Pressure	Piezoresistive	$\pm 0.025bar$
Pressure difference	Piezoresistive	$\pm 7.5Pa$
Mass flow rate	Coriolis	±0.1% of m. value

Table 3
Overview of the experimental studies with boundary conditions (varied parameter in bold).

No.	Heat Load	Recooling temperature	Height difference	Refrigerant/ charge
1	**50-1000W**	30-60°C	1m	R1233zd(E), 0.5kg
2	50-1000W	**30-60°C**	1m	R1233zd(E), 0.5kg
3	250-1000W	30°C	**0.76-1.16m**	R1233zd(E), 0.5kg
4	300-900W	30°C	1m	R1233zd(E), 0.**4-0.7**kg
5	100-1000W	30°C	1m	**R1233zd(E)/R1224yd(Z)**, 0.5kg

from measuring values are given in the respective captions.

3. Parameter studies

Table 3 shows an overview of the experimental studies. Each test did not begin until a steady state was reached. Then the measured values are recorded with a frequency of 1Hz over a period of 5min and averaged over time.

Contrary to pumped or compressed cycles, the operating point of a two-phase thermosyphon loop is mainly determined by the external operating conditions, since it is characterized by only one pressure level. The mass flow rate results from the momentum balance, which is composed of the pressure differences due to friction (in all parts of the system), acceleration/deceleration (in the evaporator and condenser) and gravitation (in all parts with a height difference):

$$\Delta p_{tot} = 0 = \Delta p_{fric} + \Delta p_{acc} + \Delta p_{grav} \tag{1}$$

The driving pressure difference results as part of Δp_{grav} from the difference in density between the riser and downcomer:

$$\Delta p_{drive} = (\rho_{downcomer} - \rho_{riser}) \cdot g \cdot \Delta H \tag{2}$$

$$[10pt] = \left(\rho_l - \left(\rho_l(1-\epsilon) + \rho_g \cdot \epsilon\right)\right) \cdot g \cdot \Delta H \tag{3}$$

with ϵ as the void fraction in the riser tube.

The pressure drop due to liquid friction in the pipe, which mainly occurs in the downcomer, increases potentially with the mass flow rate in the considered operating range of low turbulent Reynolds numbers according to the empirical Blasius equation:

$$\Delta p_{fric,l} = \frac{0.3164}{\sqrt[4]{Re}} \cdot \frac{L}{D} \cdot \frac{\rho \cdot u^2}{2} \tag{4}$$

The two-phase frictional pressure drop behaves in a more complex way, since it is determined additionally by the interaction between the gas and liquid phase. The main influencing factor here is the steam quality x, which directly results from the evaporator's energy balance:

$$\dot{Q}_H = \dot{m} \cdot \left(c_{pl} \cdot \Delta T + x \cdot h_{fg}\right) \Leftrightarrow x = \frac{\dot{Q}_H}{\dot{m} \cdot h_{fg}} - \frac{c_{pl} \cdot \Delta T}{h_{fg}}, \tag{5}$$

where ΔT is the subcooling of the refrigerant. Despite the difficult modeling of two-phase flows with corresponding differences in the calculated pressure drops, all well-known models like Friedel (1979) or Müller-Steinhagen and Heck (1986) show a potential increase with the mass flow rate and an approximately linear increase with the steam quality for the range of $x = 2 - 60\%$ occurring in this test setup.

Pressure differences due to acceleration or deceleration result from the conversion between static pressure and kinetic energy and can therefore be calculated from the momentum conservation as follows:

$$\Delta p_{acc} = \frac{\dot{G}^2}{\rho_l} \cdot \left\{ \underbrace{\left[\frac{(1-x_o)^2}{(1-\epsilon_o)} + \frac{\rho_l \cdot x_o}{\epsilon_o \cdot \rho_g}\right]}_{condenser:\ \rightarrow\ 1\ (x_o=0)} - \underbrace{\left[\frac{(1-x_i)^2}{(1-\epsilon_i)} + \frac{\rho_l \cdot x_i}{\epsilon_i \cdot \rho_g}\right]}_{evaporator:\ \rightarrow\ 1\ (x_i=0)} \right\} \tag{6}$$

With complete condensation, one term simplifies for the evaporator and the condenser respectively. It should be noted that pressure differences due to acceleration/deceleration only have to be taken into account for individual components but not for the whole system, since they add up to zero over the closed loop, similarly to changes in the cross-sectional area.

As the void fraction

$$\epsilon = \frac{A_g}{A_g + A_l} = \frac{1}{1 + \frac{u_g}{u_l} \cdot \frac{1-x}{x} \cdot \frac{\rho_g}{\rho_l}} \tag{7}$$

occurring in Eq. (3) and (6) depends on the slip ratio between the liquid and gas phase, a second empirical equation is required besides the frictional pressure drop to calculate the momentum balance (Thome (2016)). In this study the well-known correlation of Rouhani and Axelsson (1970) based on the drift-flux model is used:

$$\epsilon_{Rouhani} = \left(\frac{C_0}{\epsilon_{hom}} + \frac{\rho_g \cdot u_{gi}}{x \cdot \dot{G}}\right)^{-1} \tag{8}$$

with

$$C_0 = 1 + 0.2 \cdot (1-x) \cdot \frac{(g \cdot D_h)^{0.25} \cdot \rho_l^{0.5}}{\dot{G}^{0.5}} \tag{9}$$

$$[10pt] u_{gi} = 1.18 \cdot \left(g \cdot \sigma \cdot \left(\rho_l - \rho_g\right)\right)^{0.25} \cdot (1-x) \cdot \rho_l^{-0.5} \tag{10}$$

and ϵ_{hom} as the homogeneous void fraction with $u_g = u_l$ in Eq. (7).

The boundary conditions which have a significant influence on the determining equations shown above are considered in detail below.

3.1. Heat load and recooling temperature

In a refrigeration cycle without a pump or compressor, the one pressure level (and thus also the basic temperature level) is determined by the outer temperature at the heat sink. This temperature also sets the refrigerant properties accordingly. In this work it is defined as the

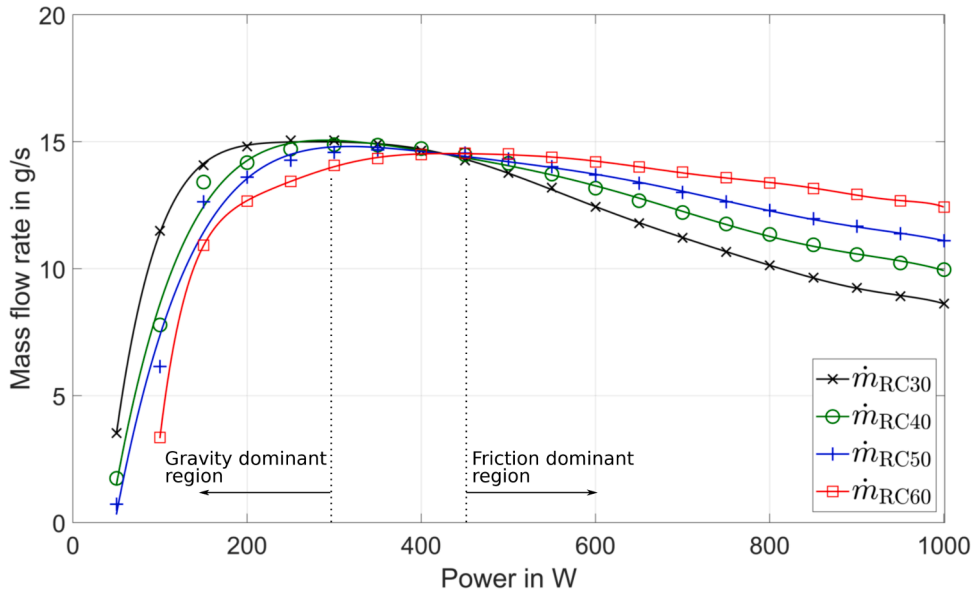

Fig. 3. Mass flow rate as a function of the heat load at different recooling temperatures.

recooling temperature at the condenser outlet, since the heat transfer between the condensing refrigerant and the actual heat sink (e.g. ambient air) is not part of the investigated system. The power of the heating cartridges equals the introduced heat load and thus determines the evaporator's energy balance (Eq. (5)). Figure 3 shows the measured mass flow rate over the heating power for different recooling temperatures.

The curves result from the pressure differences within the thermosyphon loop shown in Fig. 4.

The gravitational part of the pressure difference across the downcomer is the driving force of the system and the positive part of Δp_{drive} in Eq. (2). It is determined by the recooling temperature and liquid filling of the tube, since it only depends on the mean density. As can be seen, the pressure difference rises due to an increasing filling level of the downcomer tube, as the refrigerant mass accumulates on this side of the loop for higher heat loads. At high power, the curve begins to converge towards a maximum, as the pipe is fully filled up with liquid to the condenser outlet. The superimposed, relatively low, liquid frictional pressure drop remains approximately constant in accordance with the mass flow from an output of around 200W. At a higher recooling temperature, there is a lower liquid density, which leads to lower hydrostatic pressures. Since a lower density results in a higher filling of the downcomer tube from lower power on and in a less rising pressure with increasing filling, the curve shown is flatter.

The pressure differences across the evaporator and riser tube are negative but shown here as absolute values. Because of the low mass flux and vapor quality, Eq. (6) gives values below 300Pa for the pressure difference due to acceleration in the evaporator, which is negligible compared to the others. As the evaporator has a low height and the hydrostatic pressure is dominated by the constantly liquid-filled bottom part, the curve shown is determined by friction. Taking the above mentioned models as a basis for the two-phase frictional pressure losses, the increasing measured value in the lower power range results from the strong increase in mass flow rate, superimposed with an approximately linear increase in the vapor quality (see Fig. 5).

At high heat loads, the curve of the pressure difference across the evaporator flattens due to the decreasing mass flow rate. For higher recooling temperatures, the corresponding rising pressure in the system leads to compression of the gas phase and an associated strong increase in density. As a result, the two-phase frictional pressure drop at a recooling temperature of 60°C is significantly lower than at 30°C, with the difference increasing with power.

Since the superposition of the pressure difference components across the riser tube is more complex, they are plotted separately together with

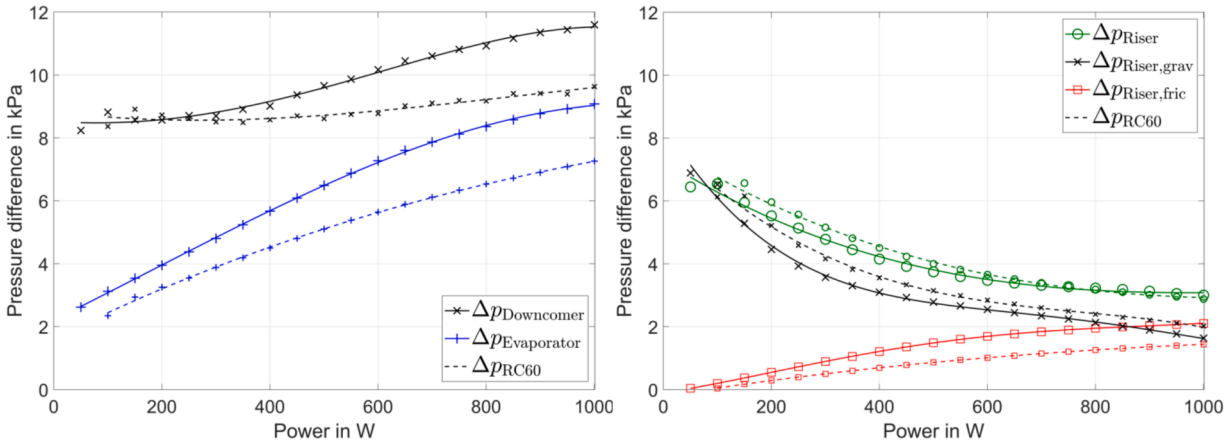

Fig. 4. Absolute pressure differences across the downcomer and evaporator (total) as well as the riser (total, gravitational, frictional) as a function of the heat load at different recooling temperatures.

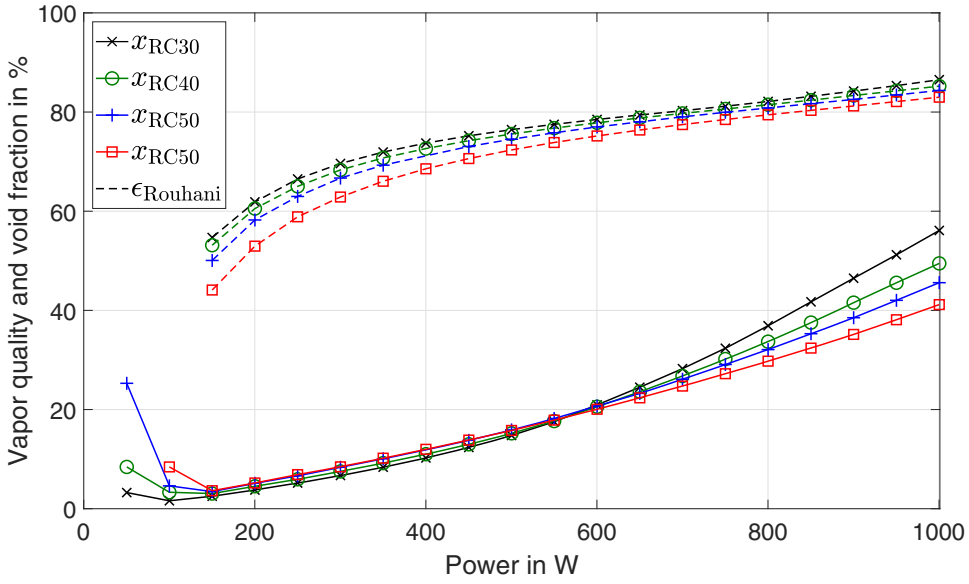

Fig. 5. Vapor quality and volumetric void fraction (Eq. (8)) at the evaporator outlet as a function of the heat load at different recooling temperatures. (Max. uncertainty: $x \pm 0.08\%, \epsilon \pm 0.3\%$)

the total measured values in Fig. 4 (right). The gravitational pressure difference is calculated using the void fraction model of Rouhani (Eq. (8)), which is shown in Fig. 5. Comparing the respective courses at a recooling temperature of 30°C, $\Delta p_{\mathrm{Riser,grav}}$ shows a reverse curve to ϵ according to Eq. (3). The frictional pressure drop in the riser tube shown in Fig. 4 is calculated using the model of Müller-Steinhagen and Heck (1986) and shows a curve similar to the evaporator, with lower values due to the simple tube geometry. Both parts add up to a decreasing total pressure difference converging towards a value of about 3000Pa with an increasing proportion of two-phase frictional pressure losses at higher heat loads.

Setting up the pressure balance by subtracting the pressure drops across the evaporator and riser from the positive pressure difference across the downcomer results in the mass flow rates shown in Fig. 3. Due to the strongly rising void fraction and associated decrease of the hydrostatic pressure in the riser tube with low frictional pressure drops at the same time, the mass flow rate shows a strong increase in the lower power range, followed by a maximum value. The driving pressure difference is progressively compensated for by frictional pressure drop in the two-phase flow, resulting in a slightly decreasing mass flow rate at higher heat loads. Therefore, the operating range of the system can be devided into a gravity dominant and a friction dominant region. At a higher recooling temperature, both the driving pressure differences as well as the frictional pressure losses show less dynamic and lower values. Thus the mass flow rate rises more slowly with a less significant maximum shifting to higher heat loads and a much smaller subsequent decrease compared to the corresponding values at low recooling temperatures. The almost constant mass flow rate over a wide range of heat loads indicates a more stable system behavior due to the higher operating pressure.

The increased values of the vapor quality for very low power shown in Fig. 5 are the consequence of DWI type I instability for low pressure TPLTs described by Nayak and Vijayan (2008).

The overall thermal resistance is an appropriate quantity to evaluate the influence of the heat load and recooling temperature on the cooling performance of the loop thermosyphon. It is composed of the heat load and the sum of the resulting individual temperature differences between the heat source and the heat sink:

$$R_{\mathrm{th}} = \frac{\sum \Delta T_{\mathrm{i}}}{\dot{Q}_{\mathrm{H}}} \tag{11}$$

The temperature difference between the evaporator wall surface and the refrigerant at the condenser outlet is used here, taking the boiling heat

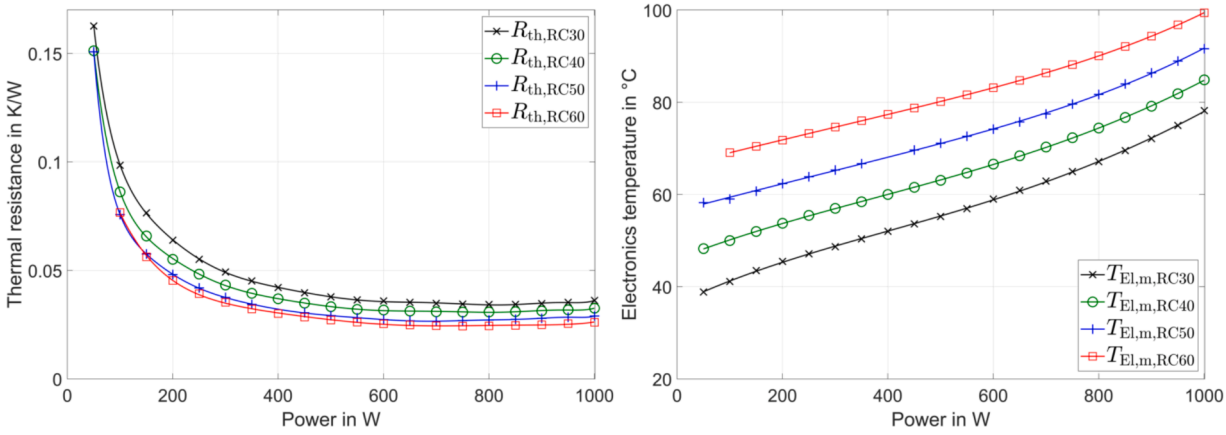

Fig. 6. Overall thermal resistance of the TPLT and mean temperature at the electronics surface as a function of the heat load at different recooling temperatures. (Max. uncertainty: $R_{\mathrm{th}} \pm 0.067 K/W$).

transfer and the heat transfer of the two-phase flow between the evaporator and condenser into account. The resulting values are shown in Fig. 6.

Since the temperature difference of the flowing refrigerant between condenser and evaporator equals the subcooling, which only slightly rises with the heat load, the thermal resistance along the loop strongly decreases and is relatively low from a power of 100W. The temperature difference between the saturated vapor and the evaporator surface equals the wall superheating, which for subcritical nucleate boiling mainly depends on the heat flux, mass flux, saturation pressure as well as the evaporator's geometry and surface condition (Stephan et al. (2017)). In the lower power range the boiling thermal resistance decreases with the strongly rising mass flux, followed by almost constant values due to the compensation between both the linearly rising heat load and resulting heat transfer coefficient. From a power of 400W the overall thermal resistance appears as almost constant, low values between 0.03K/W and 0.05K/W, with better performance for higher pressure and recooling temperature respectively.

The mean temperature on the electronics surface as the target parameter of the considered system shown in Fig. 6 (right) results from the recooling temperature and the sum of the individual temperature differences between the electronics and the condenser. Compared to the above-mentioned thermal resistance, here the conduction between the evaporator wall and the electronics has to be considered, which leads to a linear increase of the achievable temperatures at the component to be cooled. The electronics temperature increases by about 8K when the recooling temperature is increased by 10K, showing the improvement in system performance with higher system pressure. On the whole, it can be seen that the main temperature increase and therefore the main potential for optimization occurs in the evaporator assembly and not the TPLT, which offers the opportunity to fall back on widely used methods to improve the cooling performance.

3.2. Height difference between evaporator/condenser

The driving pressure difference of a TPLT depends on the height of the liquid column in the downcomer tube (Eq. (2)). As shown in the previous section, for a refrigerant charge of 0.5kg the downcomer tends to be fully filled with liquid at higher heat loads. Therefore the constructive height difference between the condenser and evaporator is a parameter of interest when designing a TPLT. Figure 7 shows the mass flow rates and electronics temperatures resulting from height differences between 0.76m and 1.16m.

Due to an increasing driving pressure difference the mass flow rate increases with the height difference by about 1g/s per 10cm for a heat load of 500W. The corresponding electronics temperature remains almost constant, since the varying mass flow rate is compensated for by an adapting vapor quality, showing the beneficial self-regulation of a well-designed TPLT. For a heat load of 1000W, the increase in mass flow rate is lower with a value of about 0.6g/s per 10cm, as the absolute two-phase frictional pressure losses are much higher (see Section 3.1). Here, the achievable temperatures are increasingly affected by decreasing height differences, as the system operates at higher vapor qualities tending towards superheating of the gas phase. This also shows that operating the system with a sufficient distance from complete evaporation of the refrigerant is advantageous.

3.3. Refrigerant charge

In contrast to refrigeration cycles with two pressure levels, subcooling as well as evaporation to the dry-out point and beyond is undesirable in loop thermosyphons. Thus the refrigerant charge or rather filling level is an important parameter when looking at TPLTs. In Fig. 8 the mass flow rate is shown as a function of the refrigerant charge for different heat loads. At charges below 0.5kg the downcomer tube of the investigated system is only partially filled with liquid, especially at low power, resulting in decreased mass flow rates due to lower driving pressure differences. Above 0.5kg the downcomer is fully filled with liquid and the further, less strong increase is explained by the differences between the vapor quality and the void fraction, shown in Fig. 8 (right). The vapor quality increases more sharply with decreasing charge than the void fraction, which reaches values close to 1. Since the vapor quality affects the two-phase pressure loss, whereas the void fraction affects the driving pressure difference, the losses increasingly dominate for lower refrigerant charges. This effect is more significant at higher heat loads, leading to flatter curves of the mass flow rate for low power.

As soon as the downcomer tube is fully filled with liquid, which occurs with increasing charge or heat load, the refrigerant starts to cool down below the saturation temperature (see Fig. 9).

Since the recooling temperature at the condenser outlet is the fixed temperature level in the system, this leads to a rising saturation temperature and pressure accordingly. So the subcooling directly adds up to the electronics temperature, showing an increase of 7.0K to 14.4K between 0.5kg and 0.7kg refrigerant charge in Fig. 9 (right). Looking at the portions of sensible and latent heat transfer in Fig. 10, which can be calculated separately from Eq. (5), the share of the preferred, highly

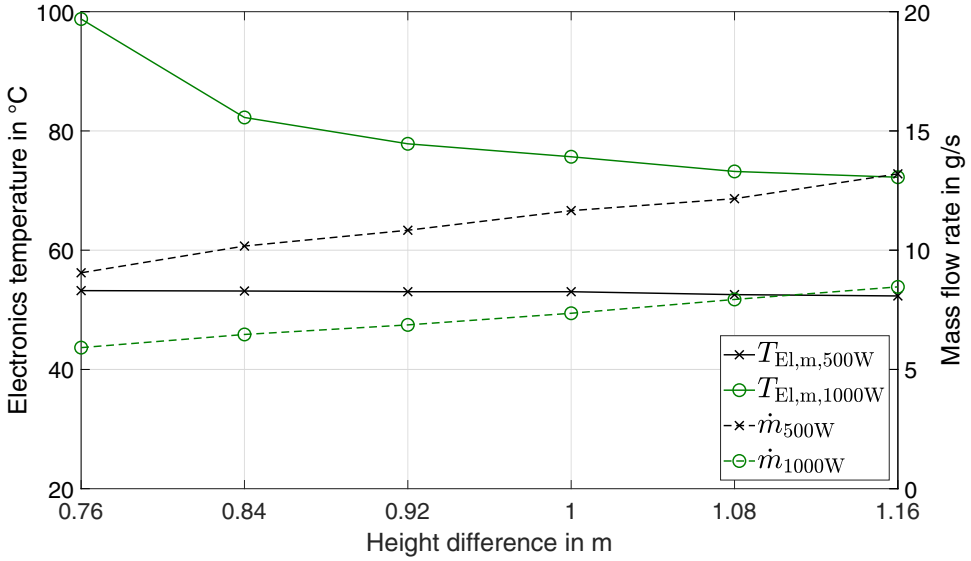

Fig. 7. Mean temperature on the electronics surface and mass flow rate as a function of the height difference between evaporator outlet and condenser inlet.

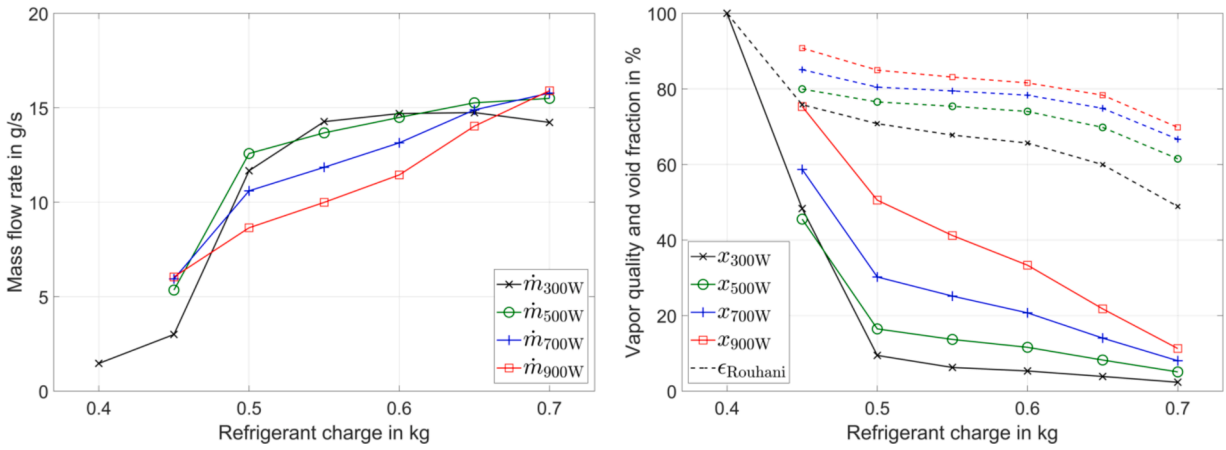

Fig. 8. Mass flow rate as well as vapor quality and void fraction at the evaporator outlet as a function of the refrigerant charge at different heat loads. (Max. uncertainty: $x \pm 0.12\%, \epsilon \pm 0.23\%$).

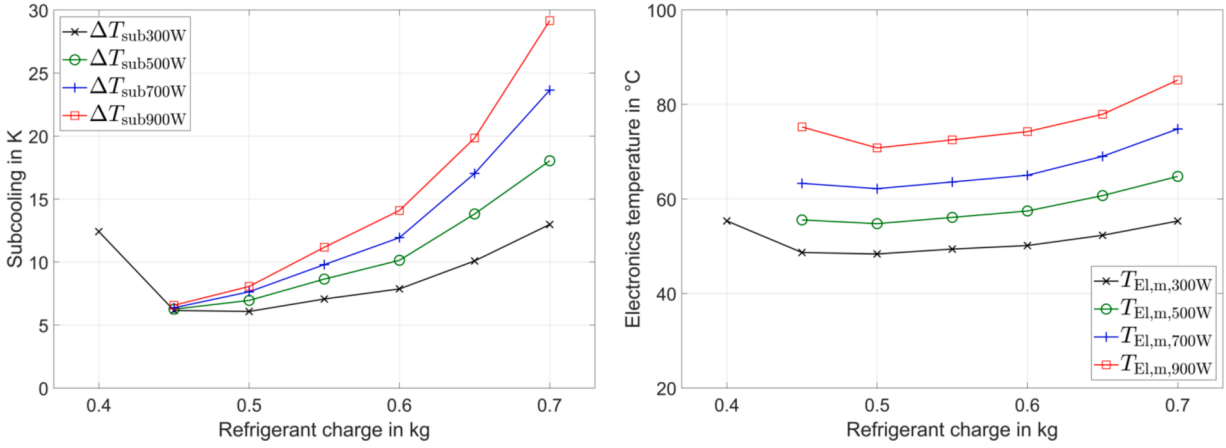

Fig. 9. Subcooling at the condenser outlet as well as the mean electronics temperature as a function of the refrigerant charge at different heat loads.

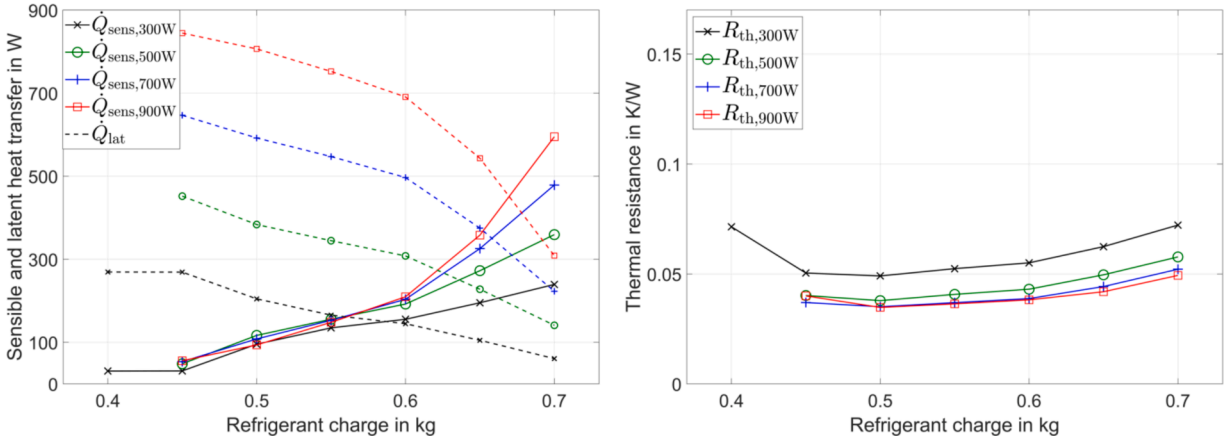

Fig. 10. Sensible and latent portion of the heat transfer as well as the overall thermal resistance as a function of the refrigerant charge at different heat loads. (Max. uncertainty: $\dot{Q}_{sens} \pm 1.36W, \dot{Q}_{sens} \pm 1.78W, R_{th} \pm 0.008K/W$).

effective latent heat transfer without temperature rise increases with decreasing refrigerant charge, reaching almost the full heat load at 0.45kg.

However, there is a lower limit here, which becomes apparent when looking at the vapor quality and void fraction again. At charges below 0.5kg these values increase sharply, indicating the beginning dry-out of the evaporator wall, which results in rising electronics temperatures. This becomes particularly clear when looking at the temperature distribution on the electronics surface in Fig. 11.

Apart from slightly lower temperatures in the bottom area due to subcooling at higher charges, there is a uniform temperature distribution for refrigerant charges above 0.45kg. At a charge of 0.4kg the dry-

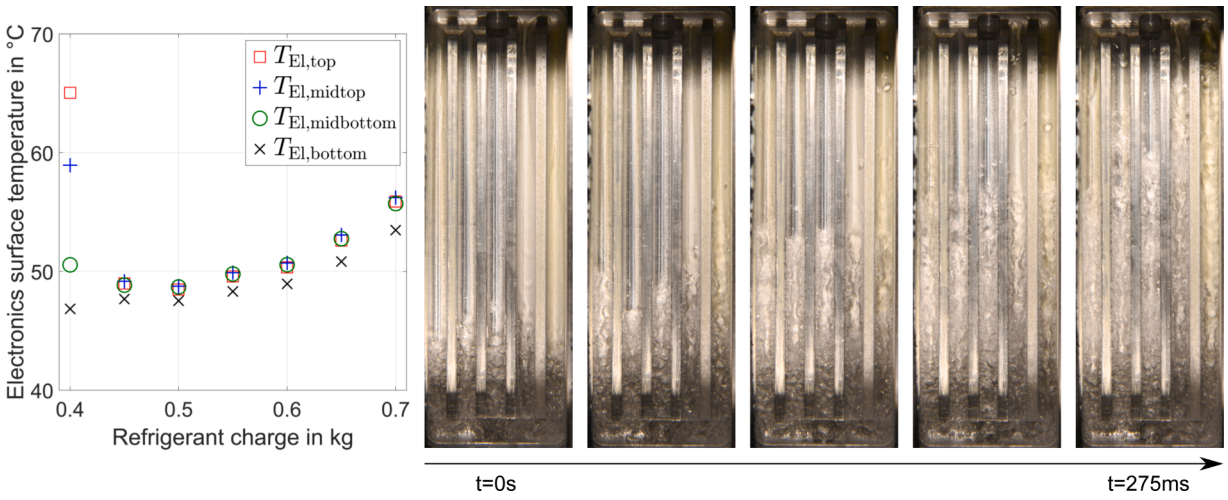

Fig. 11. Electronics surface temperature distribution at a heat load of 300W and photo sequence of oscillating flow with dry-out of the evaporator wall at a refrigerant charge of 0.4kg.

out point is already reached at the shown heat load of 300W, resulting in strong over temperature in the top evaporator and electronics area with temperature differences up to 18.2K on the surface. Due to very high local temperatures, it was not possible to carry out tests at higher heat loads at this charge. As the camera pictures of the evaporator show, the dry-out goes along with an oscillating flow. Although this oscillation with a frequency of about 0.55Hz occurs at relatively low power, it can be identified as Density-wave instability type II as defined by Nayak and Vijayan (2008). This kind of dynamic instability occurs due to the mutual feedback between mass flow rate, vapor quality and void fraction, pressure drop and density in natural circulation systems. Small flow fluctuations result in larger fluctuations of the high two-phase frictional pressure loss depending on both mass flow rate and vapor quality. These fluctuations propagate slowly in the two-phase region, unlike the fluctuations of only mass flow rate depending frictional pressure losses in the incompressible one-phase flow in the downcomer tube. When the two-phase and one-phase pressure drop fluctuations are almost of the same magnitude but opposite in phase, a sustained oscillation appears, as can be seen here.

On the whole, an optimal refrigerant charge is reached when the downcomer tube is just filled with liquid, avoiding flooding of the condenser and dry-out of the evaporator. In this system, the corresponding value is about 0.5kg. Looking at the overall thermal resistance in Fig. 10 (right), values between 0.035K /W and 0.049K /W are attainable at this charge, again showing better performance for high power. It should be noted that much of the refrigerant mass accumulates in the lower part of the system, where the pump for filling, the mass flow sensor and several fittings are located. This is why the given values for the refrigerant charge are much higher than for a system with only the essential components, and the considered range includes very low charges.

3.4. Comparison of R1233zd(E)/R1224yd(Z)

The HFO-refrigerant R1224yd(Z) is tested as an alternative working fluid for the TPLT, having a slightly higher saturation pressure, a lower enthalpy of vaporization and a higher liquid density compared to R1233zd(E) (see Table 1). Figure 12 shows the measured mass flow rates as a function of the heat load for both refrigerants.

Since the fluid properties are comparable, the mass flow rates resulting from the momentum balance show a similar curve, with the small deviations becoming clear when looking at the pressure differences in Fig. 13.

Due to the higher liquid density, the hydrostatic pressure in the

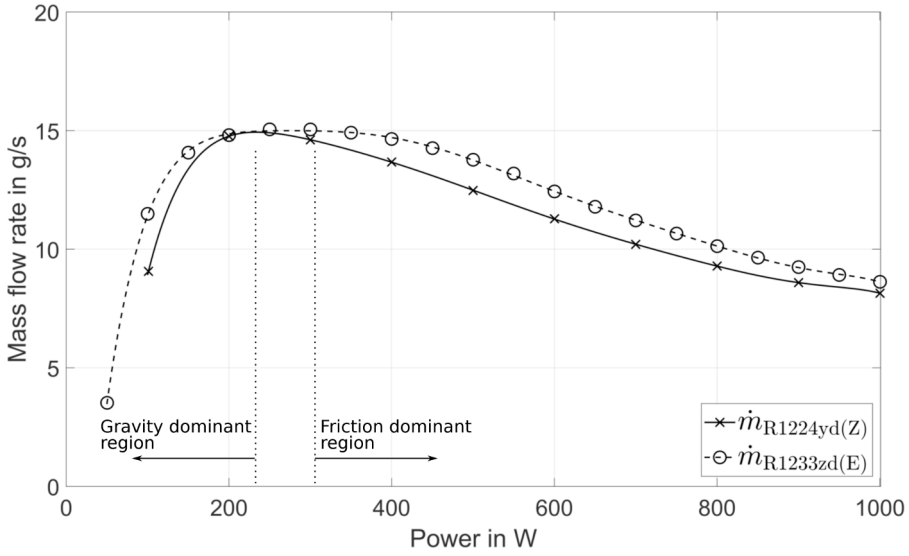

Fig. 12. Mass flow rate as a function of the heat load for R1224yd(Z) and R1233zd(E).

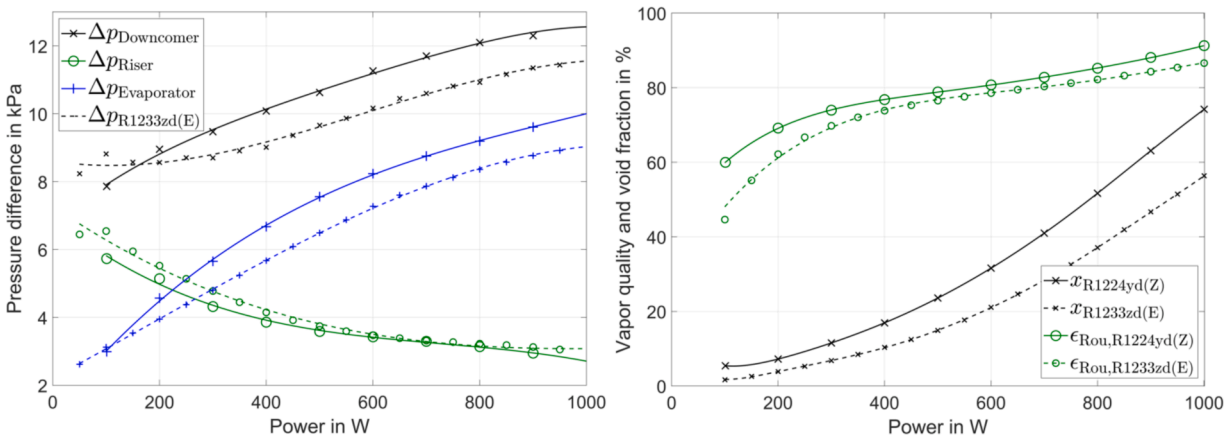

Fig. 13. Absolute pressure differences across the downcomer, riser and evaporator as well as the vapor quality and void fraction (Eq. (8)) at the evaporator outlet as a function of the heat load for R1224yd(Z) and R1233zd(E). (Max. uncertainty: $x \pm 0.09\%, \epsilon \pm 0.29\%$).

downcomer and thus the driving pressure difference is increased using R1224yd(Z). The vapor quality at same power is higher, because of the lower enthalpy of vaporization, which leads to higher frictional pressure losses in the two-phase flow in the evaporator and riser tube. Whereas this effect can be seen in the measured values of the pressure differences across the evaporator, the corresponding values in the riser tube are compensated for by lower gravitational pressure differences for a wide range of power. Overall, the two-phase frictional pressure losses in the system depending on the increased vapor quality, slightly predominate resulting in reduced mass flow rates. As shown in Fig. 13, the vapor quality and therefore the highly efficient evaporative cooling increases relatively by 32% to 226% using R1224yd(Z) instead of R1233zd(E). On the one hand, this results in a lower thermal resistance of the cooling system, as shown in Fig. 14.

The cooling performance of the TPLT with R1224yd(Z) as the working fluid is much better particularly in the range of low heat loads. On the other hand, the void fraction approaches values close to 1 at high power, with an increased risk of reaching the dry-out point in the evaporator. Looking at the electronics temperature in Fig. 14, the mean value for R1224yd(Z) exceeds the corresponding value using R1233zd (E) for heat loads above 850W. The maximum surface temperature showing higher values already above 700W indicates a beginning dry-out at the top of the evaporator.

On the whole, the refrigerant R1224yd(Z) is a good alternative for R1233zd(E), with which the cooling performance of the TPLT can even be improved in terms of the achievable thermal resistance. However, with mass flow rates that have high values over a larger power range and operation at a higher distance from the dry-out point, R1233zd(E) guarantees a more stable operation of the system.

4. Conclusions

In this study, the influence of essential internal and external operating parameters on the behavior and cooling performance of a two-phase loop thermosyphon (TPLT) is examined, using the low-GWP refrigerants R1233zd(E) and R1224yd(Z). For this purpose a test rig is build representing a TPLT and various tests in steady state are carried out to investigate the relationships between the strongly coupled loop parameters, focusing on the connection between energy and flow. The main findings can be summarized as follows:

- The **recooling or heat sink temperature** sets the basic temperature level of the system. With higher values, more stable operation with lower power-dependent dynamics and reduced thermal resistance can be achieved.
- The **heat load of the electronics** leads to stable and nearly constant mass flow rates in almost the entire range investigated, resulting in a very low, constant overall thermal resistance above medium power.
- The mass flow rate increases with the **height difference** between evaporator and condenser. At medium heat load, this is fully compensated for on the thermal side by varying vapor qualities, whereas evaporation near the dry-out point at high power leads to a significant influence on the electronics temperature.

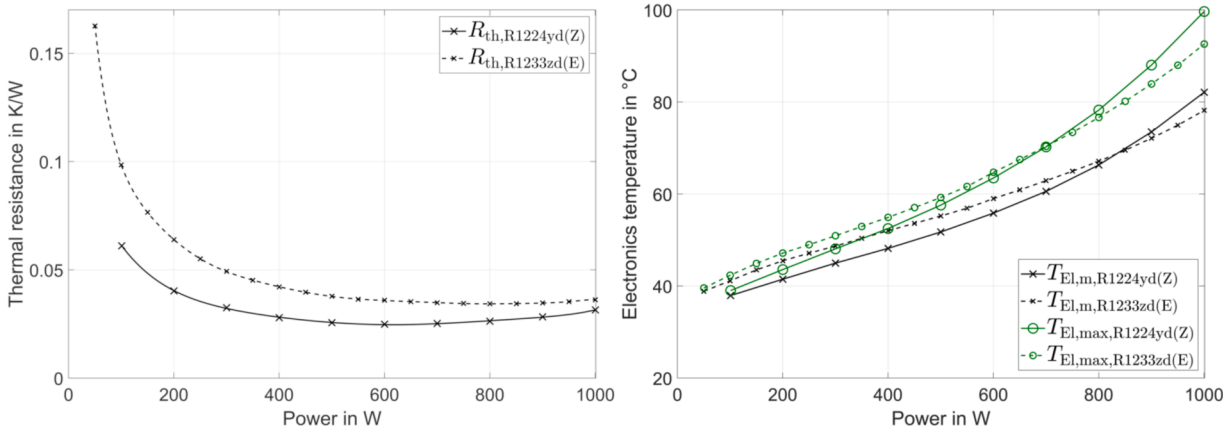

Fig. 14. Overall thermal restistance as well as mean and maximum temperature on the electronics surface as a function of the heat load for R1224yd(Z) and R1233zd (E). (Max. uncertainty: $R_{\text{th}} \pm 0.036 K/W$).

- There is an optimal **refrigerant charge**, which is obtained by reducing the filling for minimum subcooling without reaching the dry-out point in the evaporator. At charges that are too low, dry-out occurs with low frequency oscillation.
- Both tested **refrigerant alternatives** are suitable working fluids for TPLTs, with R1224yd(Z) showing better thermal performance, while R1233zd(E) results in higher system stability.

Declaration of Competing Interest

The authors declare no conflict of interest.

References

Elkholy, A., Kempers, R., 2020. Experimental investigation of geyser boiling in a small diameter two-phase loop thermosyphon. Exp. Therm. Fluid Sci. 118, 110170. https://doi.org/10.1016/j.expthermflusci.2020.110170.

Franco, A., Filippeschi, S., 2012. Closed loop two-phase thermosyphon of small dimensions: a review of the experimental results. Microgravity Sci. Technol. 24 https://doi.org/10.1007/s12217-011-9281-6.

Friedel, L., 1979. Improved friction pressure drop correlation for horizontal and vertical two-phase pipe flow. 3R Int. (18), 485–491.

Garrity, P., Klausner, J., Mei, R., 2007. A flow boiling microchannel evaporator plate for fuel cell thermal management. Heat Transf. Eng. 28, 877–884. https://doi.org/10.1080/01457630701378333.

Jouhara, H., Ezzuddin, H., 2013. Thermal performance characteristics of a wraparound loop heat pipe (WLHP) charged with R134A. Energy 61, 128–138. https://doi.org/10.1016/j.energy.2012.10.016.

Kang, S.W., Tsai, M.-C., Hsieh, C.-S., Chen, J.-Y., 2010. Thermal performance of a loop thermosyphon. Tamkang J. Sci. Eng. 13.

Khodabandeh, R., Furberg, R., 2010. Instability, heat transfer and flow regime in a two-phase flow thermosyphon loop at different diameter evaporator channel. Appl. Therm. Eng. 30 (10), 1107–1114. https://doi.org/10.1016/j.applthermaleng.2010.01.024.

Khodabandeh, R., Palm, B., 2000. An experimental and numerical investigation of pressure drop in a closed loop two phase thermosyphon system. ITHERM 2000. The Seventh Intersociety Conference on Thermal and Thermomechanical Phenomena in Electronic Systems (Cat. No.00CH37069), vol. 2, pp. 333–339. https://doi.org/10.1109/ITHERM.2000.866211.

Khodabandeh, R., Palm, B., 2002. Influence of system pressure on the boiling heat transfer coefficient in a closed two-phase thermosyphon loop. Int. J. Therm. Sci. 41 (7), 619–624. https://doi.org/10.1016/S1290-0729(02)01355-8.

Lemmon, E.W., Bell, H, I., Huber, M.L., McLinden, M.O., 2018. NIST Standard Reference Database 23: Reference Fluid Thermodynamic and Transport Properties-REFPROP, Version 10.0. National Institute of Standards and Technology. https://doi.org/10.18434/T4/1502528.

Louahlia-Gualous, H., Le Masson, S., Chahed, A., 2017. An experimental study of evaporation and condensation heat transfer coefficients for looped thermosyphon. Appl. Therm. Eng. 110, 931–940. https://doi.org/10.1016/j.applthermaleng.2016.08.111.

Milanez, F., Mantelli, M., 2010. Heat transfer limit due to pressure drop of a two-phase loop thermosyphon. Heat Pipe Sci. Technol. Int. J. 1, 237–250. https://doi.org/10.1615/HeatPipeScieTech.2011003082.

Müller-Steinhagen, H., Heck, K., 1986. A simple friction pressure drop correlation for two-phase flow in pipes. Chem. Eng. Process. Process Intensif. 20 (6), 297–308. https://doi.org/10.1016/0255-2701(86)80008-3.

Nayak, A.K., Vijayan, P.K., 2008. Flow instabilities in boiling two-phase natural circulation systems: a review. Sci. Technol. Nucl. Install. 2008 https://doi.org/10.1155/2008/573192.

Palm, B., Khodabandeh, R., 2003. Choosing working fluid for two-phase thermosyphon systems for cooling of electronics. J. Electron. Packag. 125 https://doi.org/10.1115/1.1571570.

Rouhani, S., Axelsson, E., 1970. Calculation of void volume fraction in the subcooled and quality boiling regions. Int. J. Heat Mass Transf. 13 (2), 383–393. https://doi.org/10.1016/0017-9310(70)90114-6.

Ruppersberg, J.C., Dobson, R., 2007. Flow and heat transfer in a closed loop thermosyphon Part II - experimental simulation. J. Energy Southern Africa 18, 41–48. https://doi.org/10.17159/2413-3051/2007/v18i4a3393.

VDI-Wärmeatlas. In: Stephan, P., Mewes, D., Kabelac, S., Kind, M., Schaber, K., Wetzel, T. (Eds.), 2017, Living reference work, continuously updated edition, VDI Springer Reference. Springer, Wiesbaden. https://doi.org/10.1007/978-3-662-52991-1.

Thome, J.R., 2016. Encyclopedia of two-phase heat transfer and flow I: fundamentals and methods.

Wu, C.Y., Wang, S.B., Pan, C., 1996. Chaotic oscillations in a low pressure two-phase natural circulation loop under low power and high inlet subcooling conditions. Nucl. Eng. Des. 162 (2), 223–232. https://doi.org/10.1016/0029-5493(95)01127-7.

Xu, Z., Zhang, Y., Li, B., Wang, C.-C., Ma, Q., 2018. Heat performances of a thermosyphon as affected by evaporator wettability and filling ratio. Appl. Therm. Eng. 129, 665–673. https://doi.org/10.1016/j.applthermaleng.2017.10.073.

Zhang, H., Shi, Z., Liu, K., Shao, S., Jin, T., Tian, C., 2017. Experimental and numerical investigation on a CO2 loop thermosyphon for free cooling of data centers. Appl. Therm. Eng. 111, 1083–1090. https://doi.org/10.1016/j.applthermaleng.2016.10.029.

Zhang, P., Wang, B., Shi, W., Han, L., Li, X., 2015. Modeling and performance analysis of a two-phase thermosyphon loop with partially/fully liquid-filled downcomer. Int. J. Refrig. 58, 172–185. https://doi.org/10.1016/j.ijrefrig.2015.06.014.

Zhang, P., Wang, B., Shi, W., Li, X., 2015. Experimental investigation on two-phase thermosyphon loop with partially liquid-filled downcomer. Appl. Energy 160, 10–17. https://doi.org/10.1016/j.apenergy.2015.09.033.

Zhang, P., Yang, X., Rong, X., Zhang, D., 2019. Simulation on the thermal performance of two-phase thermosyphon loop with large height difference. Appl. Therm. Eng. 163, 114327. https://doi.org/10.1016/j.applthermaleng.2019.114327.